V European Conference on Computational Fluid Dynamics
ECCOMAS CFD 2010
J. C. F. Pereira and A. Sequeira (Eds)
Lisbon, Portugal,14-17 June 2010

COMPUTATIONAL UNCERTAINTY IN TURBULENT FLOW SIMULATIONS: TOWARDS A NUMERICAL ERROR BAR

Dimitris Drikakis*, Filipe Inok

Department of Aerospace Sciences, Cranfield University,
Cranfield MK43 0AL, United Kingdom
*e-mail: d.drikakis@cranfield.ac.uk

Key words: Numerical uncertainty, turbulence , Large Eddy Simulation, high-order methods, jet flows

Abstract. *This paper presents a study of numerical errors associated with the simulations of turbulent flows. Four different computational methods have been employed in the framework of implicit large eddy simulation and computations have been performed for a jet flow configuration for which experimental data and direct numerical simulations are available. We show that a numerical error bar can be defined that takes into account the errors arising from the different numerical building blocks of the simulation method. In this study, the effects of different grids, Riemann solvers and numerical reconstruction schemes have been considered, however, the approach can be extended to take into account the effects of the initial and boundary conditions as well as subgrid scale modelling, if applicable.*

1 INTRODUCTION

Computational uncertainty is present in every system encompassing non-linearities and appears in many different domains of mathematics, physics and engineering[1, 2, 4]. In the context of computational fluid dynamics for turbulent flows, the uncertainty is associated with the non-deterministic nature of turbulence, which poses numerical modelling challenges with respect to the definition of initial and boundary conditions as well as the design of numerical methods for solving the fluid flow equations. Different ways to quantify numerical uncertainty in CFD have also been discussed in the past[3].

Modern numerical methods such as high-resolution and high-order schemes, consist of several numerical components (building blocks) for achieving better convergence and high-order order of accuracy in complex flows. For example, high-resolution schemes[26] encompass several steps in the discretisation of the partial differential equations, which include a Riemann solver and a numerical reconstruction scheme. The latter also contains slope/flux limiters which are used for adjusting the order of accuracy in the computational domain by taking into account the flow gradients on the local stencil. The conventional wisdom is that as the grid is further refined the results will converge to the same solution regardless the numerical schemes employed, however, in turbulent flow simulations such as in Large Eddy Simulation (LES), there is no explicit verification that the solution is grid-converged, because the computations are always under-resolved. One could argue that this may also be the case with respect to Direct Numerical Simulations (DNS) at least with reference to high-order statistics. Discussion on Policy Statement on the Control of Numerical Accuracy can also be found in previous discussion documents[4, 5, 6], including the notion of a numerical error bar[5].

This paper investigates some of the uncertainties associated with numerical methods in the framework of LES of turbulent flows. Numerical errors in the context of LES have also been discussed previously by other authors[9]. Specifically, a turbulent jet flow[38, 39] has been chosen as the benchmark case for different Riemann solvers, high-resolution and high-order methods and different levels of grid refinement, in order to comparatively demonstrate the effects of the above numerical components on the accuracy of the simulations. Comparisons are presented against experimental [39] and DNS data[38]. Jet flows are pertinent to many engineering applications, including propulsion, noise radiation, mixing effectiveness among others[8, 10, 11, 12, 41, 13, 14, 16, 17].

The results show that effects of the grid refinement can be comparable to the effects of the Riemann solver and numerical reconstruction scheme. Moreover, it is suggested that a numerical error bar approach could be adopted in turbulent flow simulations, which takes into account an envelope of results obtained by different methods (and subgrid scale models, if applicable).

2 COMPUTATIONAL METHODS

The computational study is based on the implicit large eddy simulation approach,e.g, see reviews[18, 19]. The computational fluid dynamics code CNS3D [19, 20, 21] has been employed, which has been previously applied to a wide range of flows featuring shock waves and turbulence[19, 22, 23, 24, 25, 28, 29, 30, 31] . The code solves the governing equations using a finite volume Godunov-type methods[32, 33, 26]. The inter-cell numerical fluxes are computed based on the solution to the Riemann problem using the reconstructed variables at the left and right of the cell interface. The computational code includes a library of different Riemann solvers[24]. In the present study the characteristics-based scheme (CBS)[24, 42] and HLLC approximate Riemann solver of[33] have been employed.

Higher order of accuracy is achieved using MUSCL extrapolation [35], with the fifth-order limiter proposed of[36]. The standard MUSCL extrapolation has been augmented using a low-Mach limiting scheme[37], which involves an additional stage in the reconstruction process for the velocity vector. It ensures uniform dissipation of kinetic energy in the limit of zero Mach number (M), extending the validity of the Godunov method to at least $M \approx 10^{-4}$, via a progressive central differencing of the velocity components. The formulation of the underlying governing equations is not changed, and monotonicity of the density and scalar field is maintained. Furthermore, numerical simulations have been performed using the ninth order weighted essentially non-oscillatory (WENO) method[27], which have been implemented into CNS3D and tested for a wide range of problems[25, 28, 30]. The time integration has been obtained using a three-stage total variation diminishing (TVD) Runge-Kutta method [26].

3 RESULTS

Simulations have been performed for an isothermal, round jet into a static free stream at a Reynolds number of $10,000$ based on the jet's outlet diameter and velocity ($M = 0.9$) at standard sea level temperature and pressure[38]. The velocities along the jet axis become non-dimensional with reference to the axial velocity of the jet at the geometrical center of the inflow, U_{ref}. Three computational meshes were employed comprising 5×10^5 (coarse), 10^6 (medium), and 2×10^6 (fine) cells, respectively. The boundary conditions were set up as inflow for the jet discharge and upstream of the jet exit; no-slip at the wall of the engine's nozzle and outflow (non-reflective boundary conditions) for the rest of the domain. Simulations were performed using the following numerical variants:

- The HLLC Riemann solver with the 5th-order MUSCL scheme and low-Mach limiting, henceforth labelled as 'CNS3D (HLLC)' or 'CNS3D (5th-order)'.
- The CBS Riemann solver in conjunction with the 5th-order MUSCL scheme and low-Mach limiting, henceforth labelled as 'CNS3D (CBS)'.
- The HLLC Riemann solver with the 9th-order WENO scheme, henceforth labelled

as 'CNS3D (9th-order)'.

Comparisons are presented with the DNS[38] and experimental[39] data. Figure 1 presents snapshots at different time instants of the axial velocity profile of the jet on the fine mesh.

Figure 2 shows the evolution of the standard deviation, for the different grid resolutions, converging to a statistically converged solution. Figure 3 shows the results for the axial average velocity for all grid resolutions, using the HLLC Riemann solver and 5th-order MUSCL scheme, and comparisons with the DNS and experimental data. The comparisons reveal that the medium and fine grids give similar results. Furthermore, the numerical (maximum) error was calculated as the absolute difference between the experimental results and the numerical prediction obtained from each method scaled by the corresponding experimental value. Furthermore, the standard-error-of-the-mean was calculated, which is defined by the standard deviation divided with the square root of the number of samples [40]. Table 1 shows the reduction in the absolute error and standard-error-of-the-mean with the grid refinement.

Computational grid	Maximum error	Standard-error-of-the-mean
Coarse	0.413	0.0160
Medium	0.273	0.0157
Fine	0.197	0.0102

Table 1: Numerical error reduction with grid refinement

Figure 4 shows the average velocity distribution for all simulation methods (on the medium grid) demonstrating the effects of the Riemann solver and numerical reconstruction scheme on the velocity distribution. Table 2 also shows the maximum error and the standard-error-of-the-mean.The following observations can be made:

- The CBS Riemann solver gives (slightly) better results than the HLLC.
- The 5th-order MUSCL gives slightly better results than the 9th-order WENO.
- The numerical uncertainty with respect to the errors associated with the numerical reconstruction schemes is of the same order of magnitude with the uncertainty associated with the grid size, medium vs fine grid (Table 1).

Assuming that the total error can be represented by the sum of the estimated maximum error and the standard-error-of-the-mean, a numerical error bar can be defined with respect to an averaged solution. For example, one possibility, including but not not limited to, is to obtain an average of all numerical predictions and put on top of it the numerical error bar, which represents a measure of the numerical uncertainty. Figure 5 shows the above and Table 2 presents the numerical error and the standard-error- of-the-mean for the averaged reconstructed solution (labelled as 'All') obtained from the various large eddy simulations.

Riemann solvers and numerical reconstruction schemes	Maximum error	Standard-error-of-the-mean
CNS3D (HLLC), 5th-order	0.1887	0.0152
CNS3D (HLLC), 9th-order	0.2697	0.0153
CNS3D (CBS), 5th-order	0.1549	0.0152
All	0.115	0.0152

Table 2: Numerical error for various LES simulations. The result obtained by averaging all LES solutions is labelled as 'All'.

4 CONCLUDING REMARK

Although this paper does not aim to provide an exhaustive account of the possibilities for defining the numerical error bar, it demonstrates that quantification of the numerical uncertainty requires appropriate amalgamation of the effects of all numerical building blocks that can potentially affect the numerical solution. By doing so, a numerical error bar can be defined, which provides the envelope of an achievable solution.

Future work will concentrate on mathematical and numerical analysis of the error bar in CFD, including the effects of initial and boundary conditions.

REFERENCES

[1] Mary L. Boas, Mathematical Methods in the Physical Sciences, 2nd Edition, *John Wiley and Sons*, (1983).

[2] Robert Eisberg and Robert Resnick, Quantum Physics of Atoms, Molecules, Solids, Nuclei and Particles, 2nd Edition, *John Wiley and Sons*, (1985).

[3] P.J. Roache, Quantification of uncertainty in Computational Fluid Dyamics, *Ann. Rev. Fluid Mech.*, **29**, 123-169, (1998).

[4] American Institute of Aeronautics and Astronautics, Guide for the Verification and Validation of Computational Fluid Dynamics Simulations, *AIAA*, **G-077**, (1998).

[5] G. Karniadakis, Toward a numerical error bar in CFD, *Journal of Fluids Engineering*, **117(1)**, 7-9, (1995).

[6] C.J. Freitas, Editorial Policy Statement on the Control of Numerical Accuracy, *Journal of Fluids Engineering*, **115**, 339, (1993).

[7] John D. Anderson, Jr., Modern Compressible Flow, *McGraw–Hill*, (1982).

[8] Dr C. W. Dennis, Mr P Sutton, Assessing Rocket Plume Damage to Launch Vehicles, *AIAA*, **4163**, (2005).

[9] J. Meyers, B.J. Geurts, M. Baelmans, Database analysis of errors in large-eddy simulation. *Physics of Fluids*, *Physics of Fluids*, **15(9)**, 2740–2755 (2003).

[10] Rupert Gleissl, Ronald M. Deslandes, Simulation of Missile Plumes for Aircraft Store Compatibility Assessments, *AIAA*, **54**, (2005).

[11] Rupert Gleissl, Ronald M. Deslandes, André Baeten, Assessment of Missile Plume Impact Characteristics, *AIAA*, **675**, (2007).

[12] K. D. Kennedy, B. J. Walker, M. C. DeMagistris, J. L. Papp , Tactical Missile Exhaust Plume At Angle Of Attack, *AIAA*, **3925**, (2004).

[13] G. Avital, J. Pompan, J.Macales, S. Yaniv, S. Gali, Experimental and CFD Study of Rocket Plume Effects on Missile Longitudinal Aerodynamic Stability, *AIAA*, **5196**, (2004).

[14] B. S. Massey, Mechnics of Fluids, 6th Edition, *Chapman and Hall*, (1989).

[15] L. D. Landau, E. M. Lifshitz, Fluid Mechnics, 2nd Edition, *Pergamon Press*, (1987).

[16] F.F. Grinstein, Vortex dynamics and entrainment in rectangular free jets, *J. Fluid Mech.*, **437**, 69–101 (2001).

[17] H. K. Tanna, An Experimental study of Jet Noise Part I: Turbulent Mixing Noise, *J. of Sound and Vibration*, **50**, 405–428 (1977).

[18] F.F. Grinstein, L.G. Margolin, W.J. Rider, Implicit Large Eddy Simulation: Computing Turbulent Fluid Dynamics, *Cambridge University Press*, (2007).

[19] D. Drikakis, Advances in turbulent flow computations using high-resolution methods, *Prog. Aerosp. Sci.*, **39**, 405–424 (2003).

[20] D. Drikakis, S. Tsangaris, An implicit characteristic-flux-averaging method for the Euler equations for real gases, *Int. J. Numer. Fl.*, **12**, 711–726 (1991).

[21] D. Drikakis, S. Tsangaris, On the solution of the compressible Navier-Stokes equations using improved flux vector splitting methods, *Applied Mathematical Modelling*, **17**, 282–297 (1993).

[22] J. Zoltak, D. Drikakis, Hybrid Upwind Methods for the Simulation of Unsteady Shock-Wave Diffraction Over a Cylinder, *Comput. Method. Appl. M*, **162**, 165–185 (1998).

[23] A. Bagabir, D. Drikakis, Mach number effects on shock-bubble interaction, *Shock Waves Journal*, **11**, 209–218 (2001).

[24] A. Bagabir, D. Drikakis, Numerical experiments using high-resolution schemes for unsteady, inviscid, compressible flows, *Computer Methods in Applied Mechanics and Engineering*, **193**, 4675–4705 (2004).

[25] D. Drikakis, M. Hahn, A. Mosedale, B. Thornber, Large eddy simulation using high-resolution and high-order methods, *Phil. Trans. R. Soc. A*, **367**, 2985–2997 (2009).

[26] D. Drikakis, W. Rider, *High-Resolution Methods for Incompressible and Low-Speed Flows*, Springer (2005).

[27] G.-S. Jiang, C.-W. Shu, Efficient implementation of weighted ENO schemes, *J. Comput. Phys.*, **126**, 202–228, 1996.

[28] A. Mosedale, D. Drikakis, Assessment of very high-order of accuracy in LES models, *Journal of Fluids Engineering*, **129**, 1497–1503 (2007).

[29] B. Thornber, D. Youngs, D. Drikakis, R.J.R. Williams, The influence of initial conditions on turbulent mixing due to Richtmyer-Meshkov Instability, *J. Fluid Mech.*, **129**, 1504–1513 (2010).

[30] S. Tissera, V. Titarev, D. Drikakis, Chemically Reacting Flows around a Double-cone, Including Ablation Effects, *AIAA*, **1285**, (2010).

[31] M. Hahn, D. Drikakis, Implicit Large-Eddy Simulation of Swept Wing Flow using High-Resolution Methods, *AIAA J.*, **47**, 618–629 (2009).

[32] S.K. Godunov, A finite-difference method for the computation of discontinuous solutions of the equations of fluid dynamics, *Mat. Sb.*, **47**, 271–295 (1959).

[33] E.F Toro, Riemann Solvers and Numerical Methods for Fluid Dynamics, *Springer-Verlag*, (1997).

[34] D. Drikakis, W. Rider, High-Resolution Methods for Incompressible and Low-Speed Flows, *Springer-Verlag*, (2004).

[35] B. van Leer, Towards the ultimate conservative difference scheme.IV. A new approach to numerical convection, *J. Comput. Phys.*, **23**, 276–299 (1977).

[36] K.H. Kim, C. Kim, Accurate, efficient and monotonic numerical methods for multi-dimensional compressible flows Part II: Multi-dimensional limiting process, *J. Comput. Phys.*, **208**, 570–615 (2005).

[37] B. Thornber, A. Mosedale, D. Drikakis, D. Youngs, R. Williams, An Improved Reconstruction Method for Compressible Flows with Low Mach Number Features, *J. Comput. Phys.*, **227**, 4873–4894 (2008).

[38] M. L. Shur, P. R. Spalart, M. Kh. Strelets, A. K. Travin, Towards the prediction of noise from jet engines, *Int. J. Heat and Fluid Flow*, **24**, 551–561 (2003).

[39] A. P. Morse, Axisymmetric turbulent shear flows with and with out swirling, *Ph. D. Thesis, University of London*, (1980).

[40] D. Zwillinger , Standard Mathematical Tables and Formulae, *Chapman and Hall*,(1995)

[41] Paul G. Tucker, Novel MILES computations for jet flows and noise, *Int. J. Heat and Fluid Flow*, **25**, 625–635 (2004).

[42] A. Eberle, Characteristic flux averaging approachto the solution of Euler's equations, Computational Fluid Dynamics, VKI Lecture Series, 1987.

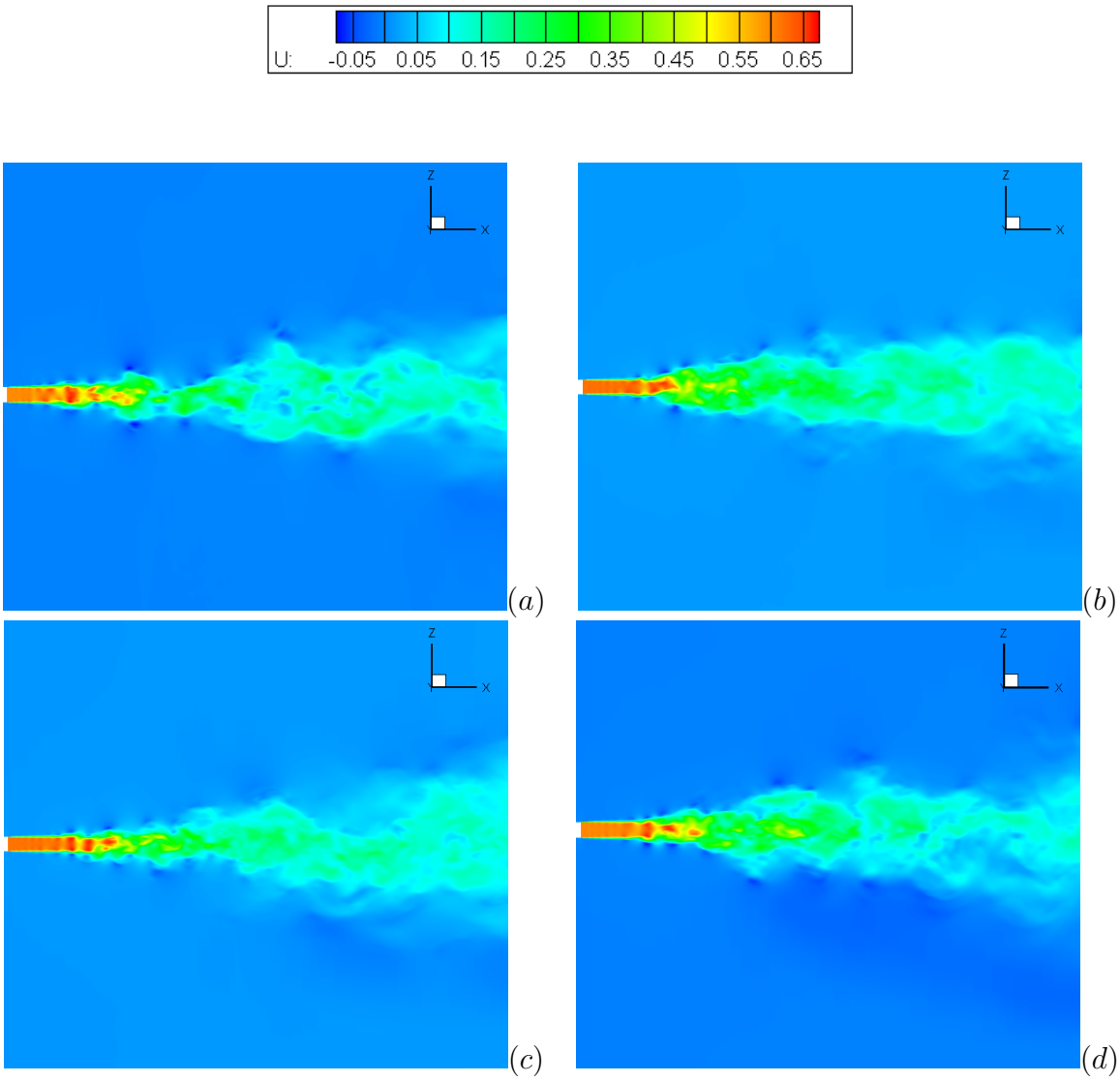

Figure 1: Instantaneous axial velocity profiles of the jet flow.(a) Initialisation, (b)after 1/3 of the simulation time, (c) after 2/3 of the simulation time and (d) at the end of the simulation.

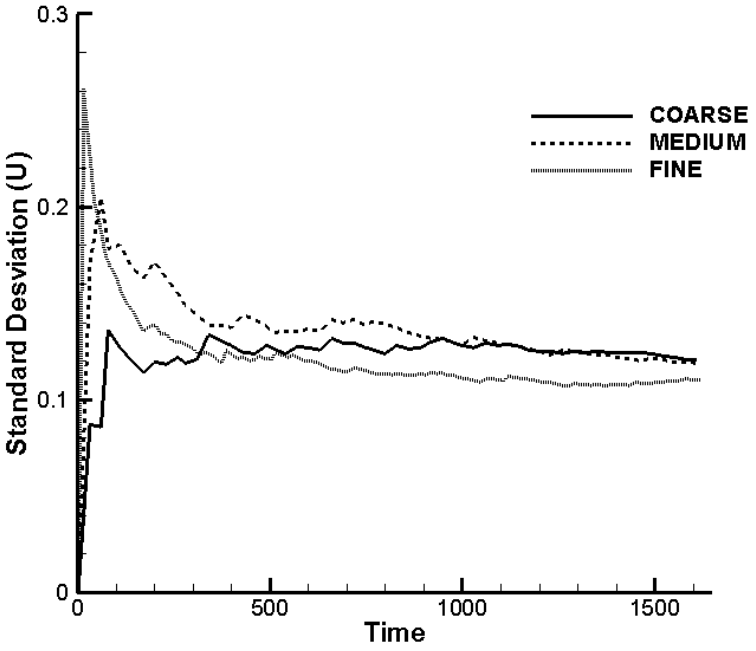

Figure 2: Maximum value of the axial velocity standard deviation along the central line for different grid resolutions.

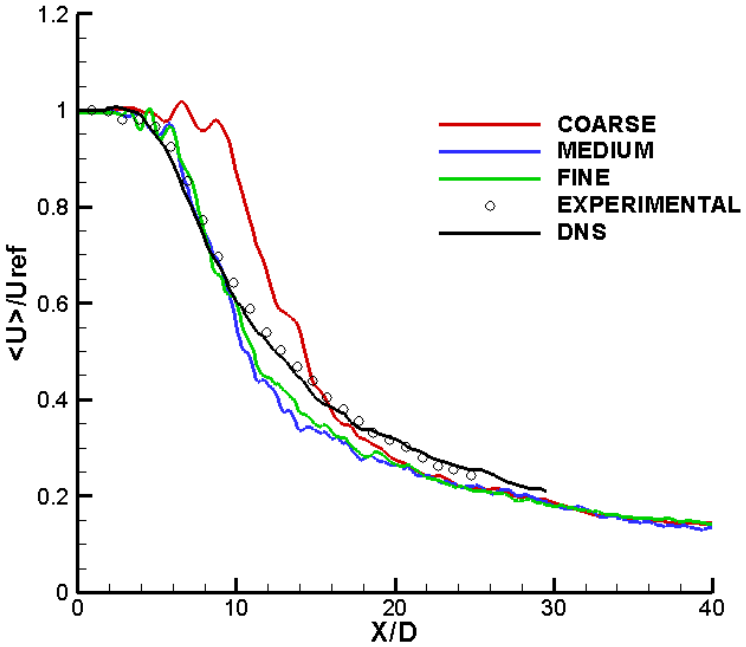

Figure 3: Comparison of the present LES predictions for the average axial velocity against DNS and experimental data.

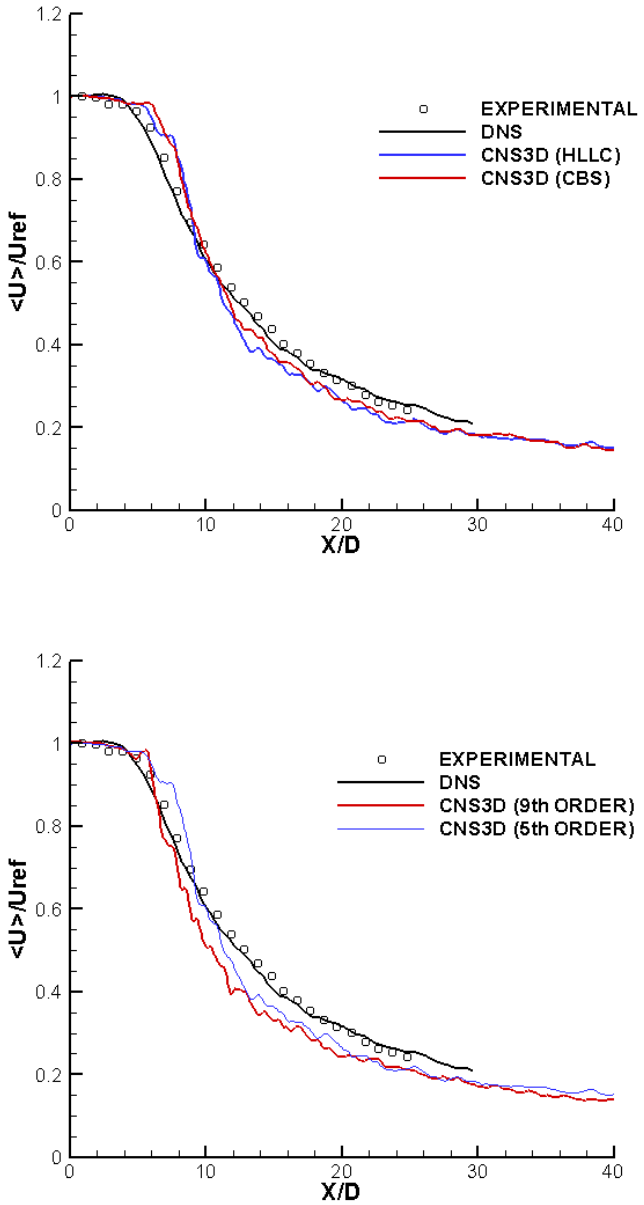

Figure 4: Effects of Riemann solver and numerical reconstruction schemes on the LES results for the average axial jet velocity distribution: HLLC and CBS Riemann Solvers (top); 9th-order WENO and 5th-order MUSCL schemes (bottom).

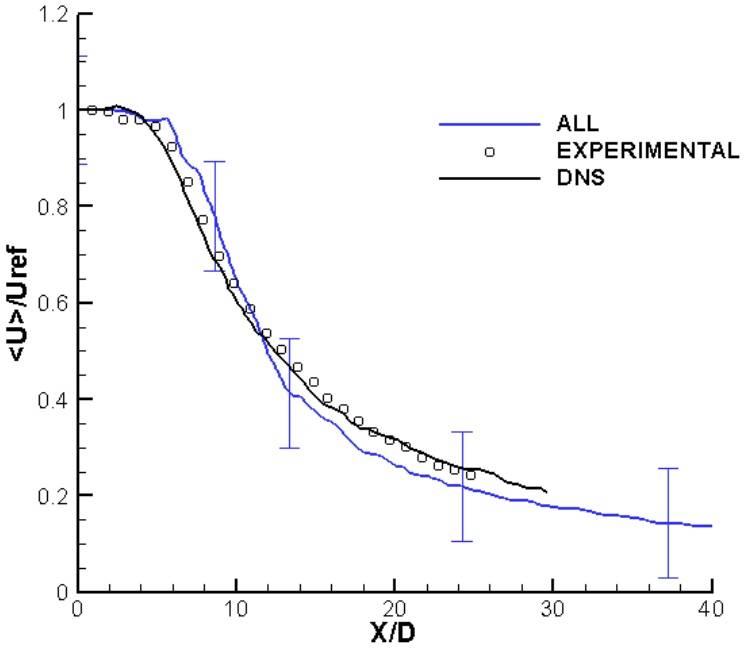

Figure 5: Average velocity distribution (labelled as 'All') obtained by averaging all LES solutions. The numerical error bar is the sum of the estimated error and the standard-error-of-the-mean.